

Exploiting Monotonicity to Design an Adaptive PI Passivity-Based Controller for a Fuel-Cell System^{*}

Carlo A. Beltrán^{*} Rafael Cisneros^{**}
Diego Langarica-Córdoba^{*} Romeo Ortega^{**}
Luis H. Díaz-Saldierna^{***}

^{*} Faculty of Sciences, UASLP, 78295 San Luis Potosí, México (emails: a332951@alumnos.uaslp.mx and diego.langarica@uaslp.mx).

^{**} Department of Electrical and Electronics Engineering, ITAM, 01080 Ciudad de México, México (emails: {rcisneros, romeo.ortega}@itam.mx)

^{***} IPICYT, 78216 San Luis Potosí, Mexico (e-mail: ldiaz@ipicyt.mx.)

Abstract: We present a controller for a power generation system composed of a fuel cell connected to a boost converter which feeds a resistive load. The controller aims to regulate the output voltage of the converter, regardless of sudden changes of the load and the fuel cell voltage. Leveraging monotonicity, we prove that the nonlinear system can be controlled by means of a simple passivity-based PI. We afterward extend the result to an adaptive version, allowing the controller to deal with parameter uncertainties. This adaptive design is based on an indirect control approach with parameter identification performed by a “hybrid” estimator, which combines two techniques: the gradient-descent and the immersion-and-invariance algorithms. The overall system is proven to be stable, with the output voltage regulated to its reference. Furthermore, realistic simulation results validate our proposal.

Keywords: Passivity-based control, Adaptive control, Power converters, Fuel cell

1. INTRODUCTION

A clean and non-intermittent source that is helping in the goal of CO₂ reduction is the fuel cell (FC). This device converts chemical energy into electrical energy with high efficiency. This conversion uses an electrochemical reaction that consumes oxygen and hydrogen to obtain electrical energy, water, and heat. Much study in recent years has focused on the proton-exchange membrane FC (PEMFC), a type of FC that stands out for its versatility, rapid start-up, and low operating temperature, among others (Ogungbemi et al., 2021). Possible applications of PEMFC are transportation electrification and microgrids. In addition, a power converter is required as an interface between the PEMFC and a DC link, forming an FC system. This electrical element routes energy from the fuel cell to the load at voltage levels compatible with the operation of the load. Consequently, advanced control algorithms are necessary to drive the operation of these devices, to ensure a tight output voltage regulation despite load changes, meeting specific dynamic responses, and having robustness against parameter uncertainties.

Furthermore, a polarization curve is the mathematical description that captures the relationship between the fuel-cell output voltage and current in steady-state. It can be characterized using empirical models that include nonlinear functions and constant parameters. To accurately

predict the operation of the fuel cell, the knowledge of these constant values is crucial. A way to determine these values is through offline estimation with data-fitting procedures, performed before the system starts its operation. However, in a real setting, these parameters are sensible to several factors such as temperature, humidity, etc. As a result of that, they change slowly while the system operation is in progress. In this regard, online estimation provides a solution to deal with these variations by continuously updating these estimates while the system operates.

In this work, we introduce a system composed of a PEMFC, a boost converter, and a load. As a control problem, the derivation of control strategies that permit the voltage regulation of the system poses a challenge due to the non-linearities describing the behavior of the FC. Besides, due to the non-minimum phase (NMP) behavior, the output voltage regulation of the boost converter is carried out indirectly, through current mode control (CMC). As widely reported, this issue is circumvented by a scheme consisting of two control loops, each one evolving in a different time scale: a “voltage” outer loop and a “current” inner loop. The rationale of this control strategy is the following. The inner control loop regulates the current to a desired reference. On the other hand, the outer loop regulates the voltage to its setpoint by providing to the inner loop the corresponding reference of the current that makes possible such task. Traditionally, the voltage loop is implemented with a PI controller,

^{*} This work has been supported by the Department of Electrical and Electronics Engineering at ITAM.

and the current loop with linear or non-linear controllers, such as passivity-based control (PBC), backstepping, and sliding mode control, among others. This scheme is applied in (Zúñiga-Ventura et al., 2018), where the current loop is designed with backstepping control. In (Beltrán et al., 2023a), the robustness of this scheme is enhanced by online estimating of the parasitic resistance of the inductor and the load conductance based on the Immersion and Invariance (I&I) (Astolfi et al., 2008). With an adaptive law, these parameters are estimated to be used in a *certainty-equivalent* way for the current control loop, designed with classic PBC. In these previous works, Lyapunov stability is demonstrated, tight voltage regulation is obtained, and the PEMFC is modeled with a two-term power function with their parameters estimated with offline data fitting procedures. A simplified scheme using a single control PI loop, based on passivity, is presented in (Cisneros et al., 2023). Offline estimation of the PEMFC parameters and online estimation of the load is performed to compute the equilibrium points required by the proposed controller. This approach exploits the monotonic nature of the polarization curve to design the controller. Relying on this property practical stability of the system operation is proven for the joint operation of the controller with the estimator. In this work, an improvement of the previous contribution is presented (Cisneros et al., 2023; Beltrán et al., 2023b). This is done by adding the gradient-descent (online) algorithm (Sastry and Bodson, 2011)—a standard approach in engineering applications—to estimate the FC parameters. The algorithm operates simultaneously with an I&I algorithm, which estimates the converter parameters. This enables the online estimation of the equilibrium point. Besides, in this note, it is also proven exponential stability of the controller when all parameters are known and asymptotically stability of the overall adaptive system. Finally, we remark that as far as authors' knowledge, there is no previous work in literature where the FC polarization curve is estimated online in closed-loop operation.

The rest of the paper is organized as follows. Section 2 presents the FCS under study and introduces the PI-PBC assuming the parameters are known. Then, in Section 3, this controller is turned adaptive with an online estimator based on I&I and gradient-descent theory. Numerical results of the closed-loop performance for the switched system are presented in Section 4. Finally, in Section 5, the conclusions of the results are presented and suggestions for further research are provided.

Notation. I_n is the $n \times n$ identity matrix. Given a full-rank matrix $G(x) \in \mathbb{R}^{n \times m}$, with $n \geq m$, we denote its left annihilator $G^\perp(x) \in \mathbb{R}^{m \times n}$ which satisfies the product $G^\perp G = 0$. When clear from the context the arguments of the functions are omitted.

2. SYSTEM DESCRIPTION AND PRELIMINARY RESULTS

The electrical circuit of the fuel cell system under consideration is given in Fig. 1. As can be seen from the figure, the system is composed of a PEMFC which feeds a load through a boost DC-DC converter. Note that a coupling capacitor C_{fc} is used between the FC and the boost converter. The converter regulates the output voltage to

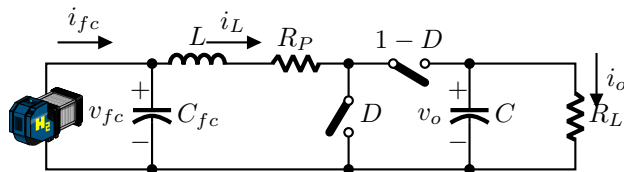


Fig. 1. System under consideration.

which the load is connected. This voltage has to be kept constant at a desired level regardless of how much power is being consumed by the load within its range of operation.

The model of the system in Fig. 1 is represented by the equations (Beltrán et al., 2024; Cisneros et al., 2023)

$$C_{fc} \dot{v}_{fc} = i_{fc} - i_L, \quad (1a)$$

$$L \dot{i}_L = -R_p i_L + v_{fc} - (1-D)v_o, \quad (1b)$$

$$C \dot{v}_o = -R_L v_o + (1-D)i_L, \quad (1c)$$

where C_{fc} and C are the coupling fuel-cell capacitor and output converter capacitor, respectively. L is the converter inductance, R_p is the inductor parasitic resistance, and R_L is the load resistance. The signal $D \in (0, 1)$ corresponds to the converter duty cycle. On the other hand, v_o is the capacitor output voltage, whereas v_{fc} and i_{fc} are the fuel-cell voltage and current, respectively. These two last variables relate to one another employing the algebraic relation (Zúñiga-Ventura et al., 2018)

$$I_{fc}(v_{fc}, \theta_s) := i_{fc} = \left(\frac{E_{oc} - v_{fc}}{\theta_{s1}} \right)^{\frac{1}{\theta_{s2}}}, \quad (2)$$

where $E_{oc} \geq 0$ refers to the open-circuit voltage of the fuel cell. Also, the parameters θ_{s1} and θ_{s2} are positive. These two constants form the vector $\theta_s := \text{col}(\theta_{s1}, \theta_{s2})$ which is included as an argument in the function for convenience. A simpler model than the well-known Larminie–Dicks model. It requires fewer parameters and the relationship between voltage and current is invertible. According with the physics of the system, i_{fc} and v_{fc} satisfy these two conditions (Dicks and Rand, 2018):

- P1. i_{fc} and v_o are non-negative.
- P2. v_{fc} is non-negative and satisfies $E_{oc} - v_{fc} > 0$.

Therefore, P1 and P2 are standing assumptions throughout this note.

Fact 1. The current and voltage in the function $-I_{fc}(v_{fc}, \cdot)$ relate in a strongly monotonic manner. Namely, for a and $b \in \mathbb{R}$ satisfying P2, there exists a constant $\alpha > 0$ such that the following inequality holds

$$(a - b) \left[-I_{fc}(a, \cdot) - [-I_{fc}(b, \cdot)] \right] \geq \alpha (a - b)^2, \quad (3)$$

Proof. The derivative of $-I_{fc}$ with respect to v_{fc} is

$$\frac{d}{dv_{fc}} [-I_{fc}(v_{fc}, \cdot)] = \frac{1}{\theta_{s2}} \left(\frac{E_{oc} - v_{fc}}{\theta_{s1}} \right)^{\frac{1}{\theta_{s2}} - 1},$$

which is positive, proving the claim.

We now replace (2) into (1a). The resulting equations (1) can be equivalently written as follows.

Fact 2. The FCS system in (1) can be represented by the dynamical system

$$Q \dot{x} = [J_0 + J_1 u - R]x + d(x_1), \quad (4)$$

where $u := 1 - D$,

$$x := \begin{bmatrix} v_{fc} \\ i_L \\ v_o \end{bmatrix}, Q := \begin{bmatrix} C_{fc} & 0 & 0 \\ 0 & L & 0 \\ 0 & 0 & C \end{bmatrix}, J_0 := \begin{bmatrix} 0 & -1 & 0 \\ 1 & 0 & 0 \\ 0 & 0 & 0 \end{bmatrix},$$

$$J_1 := \begin{bmatrix} 0 & 0 & 0 \\ 0 & 0 & -1 \\ 0 & 1 & 0 \end{bmatrix}, R := \begin{bmatrix} 0 & 0 & 0 \\ 0 & \theta_{r1} & 0 \\ 0 & 0 & \theta_{r2} \end{bmatrix}, \theta_r := \begin{bmatrix} \theta_{r1} \\ \theta_{r2} \end{bmatrix},$$

and

$$d(x_1) := \begin{bmatrix} I_{fc}(x_1, \theta_s) \\ 0 \\ 0 \end{bmatrix}, \theta := \begin{bmatrix} \theta_s \\ \theta_r \end{bmatrix},$$

where θ_{r1} and θ_{r2} are respectively the inductor parasitic resistance and the load conductance.

2.1 Assignable equilibrium points

As mentioned, the control objective is to regulate the converter output voltage x_3 to some setpoint $x_3^* > 0$. According to that, the possible closed-loop equilibrium points are given in the following lemma.

Lemma 3. The assignable equilibrium points of (4) compatible with this control objective are in the set

$$\mathcal{E} := \{x \in \mathbb{R}^3 : p(x_1, \theta) = 0, x_2 = I_{fc}, x_3 = x_3^*\}, \quad (5)$$

where

$$p(x_1, \theta) := I_{fc}(x_1, \theta_s)[\theta_{r1}I_{fc}(x_1, \theta_s) - x_1] + \theta_{r2}(x_3^*)^2,$$

Proof. Notice that (4) can be written in the affine form $Q\dot{x} = f(x) + g(x)u$ with

$$f(x) := (J_0 - R)x + d(x_1), g(x) := \begin{bmatrix} 0 \\ -x_3 \\ x_2 \end{bmatrix}. \quad (6)$$

A full-rank left annihilator of $g(x)$ is

$$g^\perp(x) = \begin{bmatrix} 1 & 0 & 0 \\ x_1 & x_2 & x_3 \end{bmatrix}.$$

The set \mathcal{E} is obtained setting $x_3 = x_3^*$ in the equation:

$$g^\perp(x)f(x) = 0.$$

2.2 The PI Passivity-based control

The proposition below defines the proposed PI-PBC for the case of known parameters $\theta := \text{col}(\theta_s, \theta_r)$. As a first approach, we assume that all parameters are known. The adaptive version is later presented where these parameters are online estimated. In both the full-information PI-PBC and its adaptive extension we assume the following.

Assumption 1. x and i_{fc} are measurable.

Lemma 4. Consider the FCS modeled by (4). Assume that all the parameters are known. Fix a desired, constant value for x_3 as $x_3^* > 0$ and compute from \mathcal{E} the associate equilibrium vector x^* . Assume that P1 and P2 hold. Consider the PI-PBC

$$\dot{x}_c = y_N(x), \quad (7a)$$

$$u = -K_P y_N(x) - K_I x_c, \quad (7b)$$

where the input signal to the PI is defined as

$$y_N(x) = x_2^* x_3 - x_3^* x_2. \quad (8)$$

For all arbitrary positive constants K_P and K_I we have that all signals remain bounded and the convergence

$$\lim_{t \rightarrow \infty} \begin{bmatrix} x(t) \\ x_c(t) \end{bmatrix} = \begin{bmatrix} x^* \\ x_c^* \end{bmatrix},$$

is *exponential*, where $x_c^* = -K_I^{-1}u^*$ with u^* the constant control associated to the equilibrium x^* .

Proof. We first show that the system is stable. It follows modifying the proof of (Hernández-Gómez et al., 2010, Prop. 2) to include the presence of the term I_{fc} and then invoking the monotonicity of Fact 1—for this reason, the procedure is only sketched. We then prove exponential stability. For, we proceed as in (Zonetti et al., 2022).

From (4) we obtain the error dynamics

$$Q\dot{\tilde{x}} = [J_0 + J_1(\tilde{u} + u^*) - R](x^* + \tilde{x}) + d(x_1) \pm d(x_1^*), \\ = (J_0 + J_1 u - R)\tilde{x} + J_1 x^* \tilde{u} + d(x_1) - d(x_1^*),$$

where $\tilde{() := () - ()^*$ and we use the equilibrium equation

$$(J_0 + J_1 u^* - R)x^* + d(x_1^*) = 0,$$

to get the third identity. Now, we notice from (8) that the passive output y_N may be written as

$$y_N = x^\top J_1 x^*,$$

and moreover that $y_N(x^*) = 0$, hence

$$y_N(x) = y_N(\tilde{x}) = \tilde{x}^\top J_1 x^*.$$

Consider the Lyapunov function candidate

$$V(\tilde{x}, \tilde{x}_c) = \frac{1}{2} \tilde{x}^\top Q \tilde{x} + \frac{K_I}{2} \tilde{x}_c^2,$$

Its time derivative satisfies

$$\dot{V} = -\tilde{x}^\top R \tilde{x} + \tilde{u} y_N(\tilde{x}) + K_I \tilde{x}_c y_N(\tilde{x}) + \tilde{x}_1 [I_{fc} - I_{fc}^*],$$

where $I_{fc}^* := I_{fc}(x_1^*, \theta_s)$. From Fact 1, there exists $\alpha > 0$ such that

$$(x_1 - x_1^*) [I_{fc} - I_{fc}^*] = \tilde{x}_1 [I_{fc} - I_{fc}^*] \leq -\alpha \tilde{x}_1^2.$$

Therefore,

$$\dot{V} \leq -\tilde{x}^\top R \tilde{x} - \alpha \tilde{x}_1^2 + \tilde{u} y_N(\tilde{x}) + K_I \tilde{x}_c y_N(\tilde{x}), \\ = -\tilde{x}^\top R \tilde{x} - \alpha \tilde{x}_1^2 + (u + K_I x_c^*) y_N(\tilde{x}) + K_I \tilde{x}_c y_N(\tilde{x}), \\ = -\tilde{x}^\top R \tilde{x} - \alpha \tilde{x}_1^2 - K_P y_N^2(\tilde{x}), \\ \leq -\tilde{x}^\top \text{diag}(\alpha, \theta_{r1}, \theta_{r2}) \tilde{x} - K_P y_N^2(\tilde{x}), \\ \leq -\kappa |\tilde{x}|^2 - K_P (\tilde{x}^\top g^*)^2,$$

with $\kappa := \min(\alpha, \theta_{r1}, \theta_{r2})$ and, from (6), $g^* := g(x^*) = J_1 x^*$. We conclude that \tilde{x} and \tilde{x}_c are bounded and, consequently, \tilde{u} (and u) is also bounded. Also, from LaSalle's Invariance principle, \tilde{x} tends to zero. Moreover, the error dynamics of the closed loop are

$$Q\dot{\tilde{x}} = \begin{bmatrix} I_{fc} - I_{fc}^* - \tilde{x}_2 \\ -R_p \tilde{x}_2 + u \tilde{x}_3 \\ -R_L \tilde{x}_3 + u \tilde{x}_2 \end{bmatrix} - g^* [K_P g_\star^\top \tilde{x} + K_I \tilde{x}_c], \\ \dot{\tilde{x}}_c = g_\star^\top \tilde{x}.$$

To prove exponential convergence, we consider the following Lyapunov function

$$W(\tilde{x}, \tilde{x}_c) = V(\tilde{x}, \tilde{x}_c) + \epsilon K_I \tilde{x}^\top g_\star^\top \tilde{x}_c, \\ = \frac{1}{2} \chi^\top \begin{bmatrix} Q & \epsilon K_I g_\star^\top \\ \epsilon K_I g_\star^\top & K_I \end{bmatrix} \chi, \chi := \text{col}(\tilde{x}, \tilde{x}_c),$$

where $\chi := \text{col}(\tilde{x}, \tilde{x}_c)$ and $\epsilon > 0$ is free. The function W is positive definite iff

$$Q - \epsilon^2 K_I g_\star g_\star^\top > 0. \quad (C1)$$

The time derivative of W is

$$\begin{aligned}\dot{W} &= \dot{V} + \epsilon K_I \tilde{x}^\top g^* \dot{\tilde{x}}_c + \epsilon K_I \tilde{x}_c g_*^\top \dot{\tilde{x}}, \\ &\leq -\kappa |\tilde{x}|^2 - K_P (\tilde{x}^\top g^*)^2 + \epsilon K_I (\tilde{x}^\top g_*)^2 + \epsilon K_I \tilde{x}_c g_*^\top \dot{\tilde{x}}, \\ &= -\kappa |x|^2 - (K_P - \epsilon K_I) (\tilde{x}^\top g_*)^2, \\ &\quad + \epsilon K_I \tilde{x}_c (v^\top - K_P g_*^\top Q^{-1} g_* g_*^\top) \tilde{x} - \epsilon K_I^2 g_*^\top Q^{-1} g_* \tilde{x}_c.\end{aligned}$$

To obtain the last expression we used the fact that the product $g_*^\top \tilde{x}$ is

$$g_*^\top \tilde{x} = v^\top \tilde{x} - K_P g_*^\top Q^{-1} g_* g_*^\top \tilde{x} - K_I g_*^\top Q^{-1} g_* \tilde{x}_c, \quad (9)$$

where $v^\top := [0 \quad \frac{R_p}{L} x_3^* + \frac{x_2^*}{C} u \quad -(\frac{x_2^*}{L} u + \frac{R_L}{C} x_2^*)]$.

The inequality above can be written in the matrix form

$$\dot{W} \leq -\chi^\top M \chi,$$

where, for $w^\top := K_I (K_P g_*^\top Q^{-1} g_* g_*^\top - v^\top)$,

$$M := \begin{bmatrix} \kappa I_3 + (K_P - \epsilon K_I) g_* g_*^\top & \epsilon \frac{w}{2} \\ \epsilon \frac{w^\top}{2} & \epsilon K_I^2 g_*^\top Q^{-1} g_* \end{bmatrix}.$$

The matrix M is positive definite iff

$$\kappa I_3 + K_P g_* g_*^\top - \epsilon \left[K_I g_* g_*^\top + \frac{1}{4K_I^2} w (g_*^\top Q^{-1} g_*)^{-1} w^\top \right] > 0. \quad (C2)$$

We conclude the proof by noting that there exists a sufficiently small constant $\epsilon > 0$ satisfying (C1) and (C2). Exponential convergence follows.

3. MAIN RESULT

3.1 Estimation of θ

An estimator of θ is a dynamical system of the form

$$\begin{aligned}\dot{\eta}(t) &= \chi_\eta(t, \eta(t), x(t)), \\ \hat{\theta}(t) &= \chi_\theta(t, \eta(t), x(t)),\end{aligned} \quad (10)$$

where $\hat{\theta}$ is the estimate of θ . It is desired that

$$\lim_{t \rightarrow \infty} \hat{\theta}(t) = \theta. \quad (11)$$

Here below, an estimation algorithm for θ in (4) is proposed. This combines two estimation approaches: the I&I technique (Astolfi et al., 2008) and the gradient-descent estimator (Sastry and Bodson, 2011) techniques. More precisely, the I&I approach is employed to estimate θ_r , as designed in (Cisneros et al., 2023), whereas the LSD estimator is implemented to identify θ_s .

The next lemma introduces a linear regression equation (LRE) obtained from the polarization curve (2). This LRE is part of the estimator equations introduced below. The proof can be found in (Beltrán et al., 2024, Lemma 4).

Lemma 5. Consider the algebraic relation in (2) with known parameter E_{oc} . The next LRE holds

$$Y(t) = \phi(t) \theta_{s2}, \quad (12)$$

where

$$\begin{aligned}Y &= \mathcal{F}\{\ln(E_{oc} - x_1)\}, \\ \phi &= \mathcal{F}\{\ln(i_{fc})\},\end{aligned}$$

and the operator $\mathcal{F}\{\cdot\}$ defined as the stable, LTI filter

$$\mathcal{F} := \frac{\lambda p}{p + \lambda}, \quad \lambda > 0.$$

Before introducing the estimation algorithm, the following assumption is in order.

Assumption 2. x_2, x_3 and $\phi \notin \mathcal{L}_2$.

Proposition 1. Let the estimator (10) be composed of the following dynamics

E1. (*Estimation of θ_s*) The gradient-descent estimator:

$$\dot{\hat{\theta}}_{s2} = \gamma \phi (Y - \phi \hat{\theta}_{s2}), \quad (13a)$$

$$\hat{\theta}_{s1} = (E_{oc} - x_1) i_{fc}^{-\hat{\theta}_{s2}}, \quad (13b)$$

for a positive gain γ .

E2. (*Estimation of θ_r*) The I&I estimator:

$$\dot{r}_{I1} = -k_1 x_2 \left(x_3 u - x_1 - \frac{1}{2} k_1 L x_2^3 + r_{I1} x_2 \right), \quad (14a)$$

$$\dot{r}_{I2} = -k_2 x_3 \left(r_{I2} x_3 - x_2 u - \frac{1}{2} k_2 C x_3^3 \right), \quad (14b)$$

$$\hat{\theta}_{r1} = -\frac{k_1}{2} L x_2^2 + r_{I1}, \quad (14c)$$

$$\hat{\theta}_{r2} = -\frac{k_2}{2} C x_3^2 + r_{I2}, \quad (14d)$$

where k_1 and k_2 are positive gains.

Fulfillment of Assumption 2 ensures that the estimation error is bounded and

$$\lim_{t \rightarrow \infty} \begin{bmatrix} e_{ri}(t) \\ e_{si}(t) \end{bmatrix} = 0, \quad i = 1, 2. \quad (15)$$

where $e_{(\cdot)i} := \hat{\theta}_{(\cdot)i} - \theta_{(\cdot)i}$.

Proof. The gradient-descent estimator in (13a) is a standard estimation algorithm. Its error dynamics $e_{s2} := \hat{\theta}_{s2} - \theta_{s2}$ are

$$\dot{e}_{s2} = -\gamma \phi^2 e_{s2}.$$

Therefore, Assumption 2 implies the convergence of the error. Moreover, using (2) with $\hat{\theta}_{s2}$ instead of the actual parameter value θ_{s2} , it is possible to obtain an estimate of θ_{s1} as in (13b).

We now prove the convergence of the I&I estimator. The time derivative of the estimation error $e_{r1} := \hat{\theta}_{r1} - \theta_{r1}$ is

$$\begin{aligned}\dot{e}_{r1} &= \dot{r}_{I1} - k_1 L x_2 \dot{x}_2, \\ &= k_1 x_2 (x_1 - r_{I1} x_2 + \frac{k_1}{2} L x_2^3 - x_3 u) \\ &\quad - k_1 x_2 [-(\hat{\theta}_{r1} - \tilde{\theta}_{r1}) x_2 + x_1 - x_3 u], \\ &= -k_1 x_2 (x_3 u + \hat{\theta}_{r1} x_2) - k_1 x_2 [-(\hat{\theta}_{r1} - \tilde{\theta}_{r1}) x_2 - x_3 u], \\ &= -k_1 x_2^2 \tilde{\theta}_{r1},\end{aligned}$$

where (14c) was used to obtain the third equality. With a similar procedure, we get

$$\begin{aligned}\dot{e}_{r2} &= \dot{r}_{I2} - k_2 C x_3 \dot{x}_3 \\ &= k_2 x_3 [x_2 u - r_{I2} x_3 + \frac{k_2}{2} C x_3^3] \\ &\quad - k_2 x_3 [-(\hat{\theta}_{r2} - \tilde{\theta}_{r2}) x_3 + x_2 u], \\ &= k_2 x_3 (x_2 u - \hat{\theta}_{r2} x_3) - k_2 x_3 [-(\hat{\theta}_{r2} - \tilde{\theta}_{r2}) x_3 + x_2 u], \\ &= -k_2 x_3^2 \tilde{\theta}_{r2}.\end{aligned}$$

Again, since $x_2 \notin \mathcal{L}_2$ and $x_3 \notin \mathcal{L}_2$ by assumption, the estimation errors e_{r1} and e_{r2} converge to zero.

3.2 The proposed adaptive PI-PBC

The full-information PI-PBC of Lemma 4 depends on the equilibrium points. When parameters are available, these points are numerically computed by a root-finding procedure applied to the equilibrium equations of \mathcal{E} . On the other hand, when these parameters are unknown, a parameter estimation has to be performed. An estimate of the equilibrium point can be carried out by solving the equations of (5) that result from replacing the actual parameters with their estimate. In other words, the estimate of the equilibrium point, \hat{x}^* , belongs to the set

$$\hat{\mathcal{E}} := \left\{ x \in \mathbb{R}^3 : p(x_1, \hat{\theta}) = 0, x_2 = \left(\frac{E_{oc} - x_1}{\hat{\theta}_{s1}} \right)^{\frac{1}{\hat{\theta}_{s2}}}, x_3 = x_3^* \right\}, \quad (16)$$

where $p(\cdot, \cdot)$ has been defined in Lemma 3.

We are now in a position to enunciate our main result.

Proposition 2. Consider the closed loop of the FCS modelled by eqs (4), the parameter estimator (13)-(14) and the adaptive PI-PBC

$$u = -K_P \hat{y}_N - K_I x_c, \quad (17a)$$

$$\dot{x}_c = \hat{y}_N, \quad (17b)$$

where $K_P > 0$ and $K_I > 0$, $\hat{y}_N(x) := \hat{x}_2^* x_3 - x_3^* x_2$ and \hat{x}_2^* is estimated, invoking certainty equivalence, using (16). Under Assumptions 1 and 2, all signals remain bounded with $(x, x_c) = (x^*, K_I u^*)$ the asymptotically stable equilibrium point. As before, $x^* \in \mathcal{E}$ is the desired equilibrium state and u^* is the associated input value.

Proof. The controller (17) is a function of the form $u = \beta(x, \hat{x}_*, x_c)$. Taking $\hat{x}^* = x^* + \delta$, where δ refers to the estimation error of the equilibrium point. The error dynamics of the closed-loop system have the form

$$\begin{aligned} \dot{x} &= f_{cl}(x, \beta(x, x^* + \delta, x_c)), \\ \dot{x}_c &= g_{cl}(x, x^* + \delta). \end{aligned} \quad (18)$$

Setting $\delta = 0$ in (18) results in the system of Proposition 4 which has been proved to be exponentially stable. From Prop. 1, \hat{x}_2^* converges to x_2^* due to the certainty-equivalence assumption. It follows that $(x^*, -K_I^{-1} u^*)$ is an asymptotically stable equilibrium point (Vidyasagar, 1980, Th. 3.1).

4. SIMULATION RESULTS

In this section, numerical simulations for validating the adaptive PI-PBC, through output voltage regulation, are performed via Simulink/MATLAB. These simulations consider the switched model of the boost converter with a switching frequency of $f_{sw} = 100$ kHz. The PEMFC stack used is a Simscape/MATLAB block, having a nominal power of 1.26 kW, consisting of 42 cells, and an open-circuit voltage E_{oc} of 42.0 V. The other parameters are $C = 1.5$ mF, $C_{fc} = 50$ mF, $L = 38.63$ μ F and $\theta_{r1} = 0.083$ m Ω . The conductance θ_{r2} varies depending on the simulated scenario as introduced below. An implementation diagram of the adaptive PI-PBC is illustrated in Fig. 2. In this figure, the block labeled as ‘‘Computation of equilibria’’ receives the parameter estimate $\hat{\theta}$. From

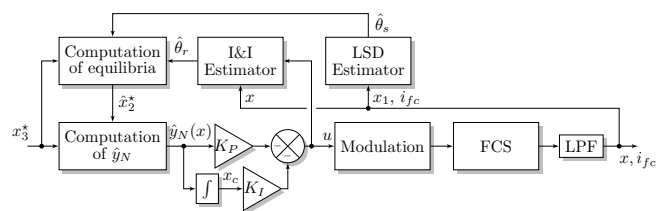


Fig. 2. Implementation diagram of the adaptive PI-PBC.

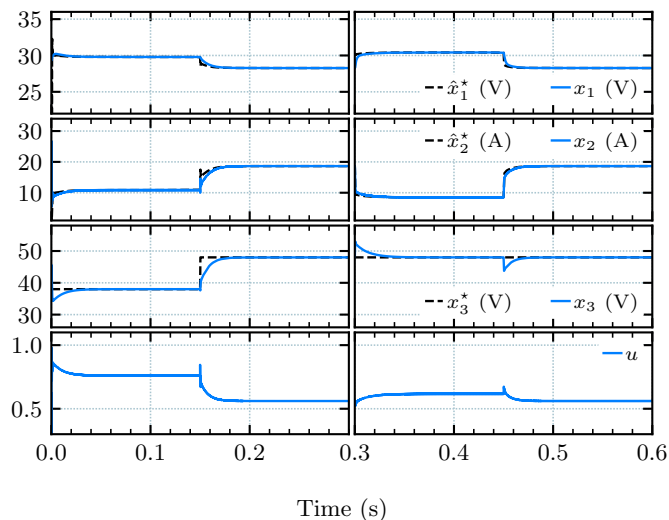
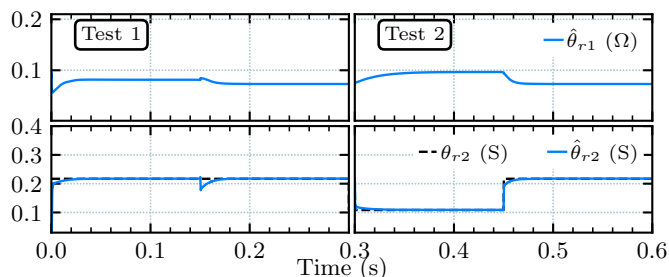


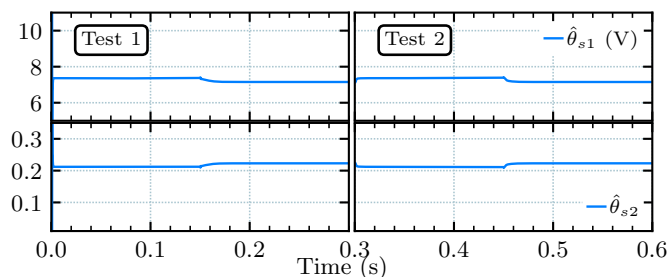
Fig. 3. Simulation results: evolution of x and u .

this vector, an estimation of the equilibrium point \hat{x}^* is computed using $\hat{\mathcal{E}}$ via the Newton-Raphson Method.

The performance of the adaptive PI-PBC is assessed under two standard scenarios. In the first test (Test 1), the output voltage regulation is evaluated when pulsating changes in the reference are performed while the load is maintained constant. A second test (Test 2) consists



(a) $\hat{\theta}_{r1}$ and $\hat{\theta}_{r2}$.



(b) $\hat{\theta}_{s1}$ and $\hat{\theta}_{s2}$.

Fig. 4. Simulation results: evolution of $\hat{\theta}_r$ and $\hat{\theta}_s$.

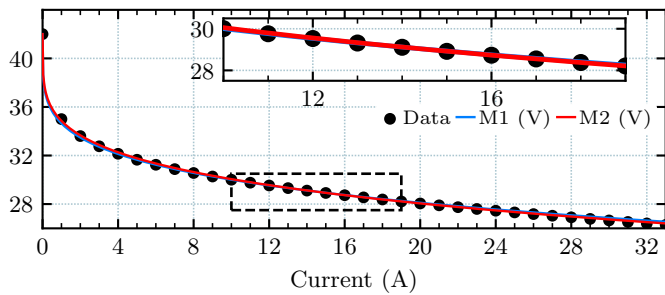


Fig. 5. Comparison of the estimated PEMFC curve with that of the MATLAB PEMFC block.

of varying the load while the voltage reference is kept constant.

As shown in Fig. 3, the resulting signals from Test 1 are plotted from $t = 0$ s to $t = 0.3$ s. Within this lapse, the load conductance $\theta_{r,2}$ is fixed at 217.0 mS, and the voltage reference pulsates between $x_3^* = 38.0$ V and $x_3^* = 48.0$ V at a frequency of 10/3 Hz. The corresponding two steady states are $x^* = (29.8$ V, 10.8 A, 38.0 V) and $x^* = (28.3$ V, 18.6 A, 48.0 V). Afterward, while the simulation is running, the test scenario is switched to Test 2. This is carried out from time $t = 0.3$ s to the stop time of simulation at $t = 0.6$ s. During this lapse, the voltage reference is fixed at $x_3^* = 48.0$ V and the $\theta_{r,2}$ pulsates between $\theta_{r,2} = 108.5$ mS and $\theta_{r,2} = 217.0$ mS at a frequency of 10/3 Hz. Inspection of Fig. 3 indicates that, during this interval of time, the output voltage is tightly regulated under pulsating changes with overshoots/undershoots of less than 5.10 V and transients of about 600 ms. The current tracks its reference, with only an appreciable difference during transients.

The evolution of the estimations can be observed in Fig. 4. Regarding $\hat{\theta}_r$, it is worth mentioning the existence of a diode and a switch on-resistances in the simulated system that are not considered in the model. These uncertainties may be compensated by $\hat{\theta}_{r,1}$ during the simulation. That is the reason why the steady state of $\hat{\theta}_{r,1}$ varies as the setpoint or load changes—see Fig. 4(a). On the other hand, $\hat{\theta}_{r,2}$ converges to the actual parameter value in each case.

Fig. 4(b) shows the convergence of θ_s . The value to which the estimates converge depends on the system state, and two pairs are distinguished in the results. At the start of Test 1, the estimations converge to $\hat{\theta}_s^* = (7.35, 0.212)$ (M1), and at the end of Test 2, the estimations converge to $\hat{\theta}_s^* = (7.15, 0.223)$ (M2). In Fig. 5, the PEMFC curve is plotted using the estimated parameters $\hat{\theta}_s$. It is compared with the values of current and voltage generated by PEMFC block during the simulation. The estimated curves, in both cases, acceptably match the current and voltage values of the PEMFC block.

5. CONCLUSIONS AND FUTURE WORK

Relying on monotonicity, we derive a PI-PBC for the fuel-cell system of eq. (4). The resulting controller has the same structure as that reported in (Hernández-Gómez et al., 2010). This approach is then extended to an adaptive version based on an indirect control scheme.

Future work is oriented to determining conditions for which our approach can be generalized to systems having the same form as that of the FCS:

$$\dot{Q}x = [J_0 - R]x + \sum_{i=1}^m (J_i x + b_i)u_i + d(x), \quad (19)$$

where $J_\ell = -J_\ell^\top$, $b_i \in \mathbb{R}^n$ and a nonlinear mapping $d : \mathbb{R}^n \rightarrow \mathbb{R}^n$ satisfying monotonicity. Doing so will enlarge the class of systems to which the PI-PBC in (Hernández-Gómez et al., 2010) is applicable—clearly, (19) encompasses the family of systems of this article.

REFERENCES

- Astolfi, A., Karagiannis, D., and Ortega, R. (2008). *Non-linear and adaptive control with applications*. Springer-Verlag, Berlin.
- Beltrán, C., Bobsov, A., Ortega, R., Langarica-Córdoba, D., Cisneros, R., and Díaz, L. (2024). Online parameter estimation of the polarization curve of a fuel cell with guaranteed convergence properties: Theoretical and experimental results. *IEEE Transactions on Industrial Electronics*, 54(2), 286–295.
- Beltrán, C.A., Díaz-Saldierna, L.H., Langarica-Córdoba, D., and Martínez-Rodríguez, P.R. (2023a). Passivity-based control for output voltage regulation in a fuel cell/boost converter system. *Micromachines*, 14, 187.
- Beltrán, C.A., Cisneros, R., Ortega, R., Díaz-Saldierna, L.H., and Langarica-Córdoba, D. (2023b). An adaptive pi-pbc approach for voltage regulation of a fuel cell based power system. In *2023 IEEE International Autumn Meeting on Power, Electronics and Computing (ROPEC)*, volume 7, 1–6.
- Cisneros, R., Ortega, R., Beltrán, C., Langarica-Córdoba, D., and Díaz, L. (2023). Output voltage regulation of a fuel cell/boost converter system: A PI-PBC approach. *International Journal of Adaptive and Control Signal Processing*, 9(39), 286–295.
- Dicks, A.L. and Rand, D.A.J. (2018). *Fuel Cell Systems Explained*. John Wiley & Sons Ltd, third edition.
- Hernández-Gómez, M., Ortega, R., Lamnabhi-Lagarrigue, F., and Escobar, G. (2010). Adaptive PI stabilization of switched power converters. *IEEE Transactions on Control System Technology*, 18(3), 688–698.
- Ogungbemi, E., Wilberforce, T., Ijaodola, O., Thompson, J., and Olabi, A. (2021). Selection of proton exchange membrane fuel cell for transportation. *International Journal of Hydrogen Energy*, 46, 30625–30640.
- Sastry, S. and Bodson, M. (2011). *Adaptive control: Stability, convergence and robustness*. Dover Publications.
- Vidyasagar, M. (1980). Decomposition techniques for large-scale systems with nonadditive interactions: stability and stabilizability. *IEEE Transactions on Automatic Control*, 25(4), 773–779.
- Zonetti, D., Bergna-Díaz, G., Ortega, R., and Monshizadeh, N. (2022). PID passivity-based control of power converters. *International Journal on Robust and Nonlinear Control*, 32(1), 1769–1795.
- Zúñiga-Ventura, Y., Langarica-Córdoba, D., Leyva-Ramos, J., Díaz-Saldierna, L., and Ramírez-Rivera, V.M. (2018). Adaptive backstepping control for a fuel cell/boost converter system. *IEEE Journal of Emerging and Selected Topics in Power Electronics*, 6, 686–695.